THE 3-D FLOW OF CASSON NANOFLUID OVER A STRETCHED SHEET WITH CHEMICAL REACTIONS, VELOCITY SLIP, THERMAL RADIATION, AND BROWNIAN MOTION

by

Muhammad UMAR[a], Zulqurnain SABIR[a], Ali IMRAN[b*], Hafiz Abdul WAHAB[a], Muhammad SHOAIB[b], and Muhammad Asif Zahoor RAJA[c]

[a] Department of Mathematics and Statistics, Hazara University, Mansehra, Pakistan
[b] Department of Mathematics, COMSATS University Islamabad, Attock Campus, Attock, Pakistan
[c] Department of Electrical and Computer Engineering, COMSATS University Islamabad, Attock Campus, Attock, Pakistan

Original scientific paper
https://doi.org/10.2298/TSCI190625339U

The 3-D flow of Casson nanofluid over a stretched sheet with chemical reactions, velocity slip, thermal radiation, and Brownian motion have been analyzed. By employing the similarity transformation, the ODE are obtained from the fluidic system PDE. The transformed ODE are handled for the numerical solution of the proposed fluidic problem by incorporating shooting technique. To compare the obtained numerical results, Lobatto 111A method has been implemented, with 5-8 decimal places of accuracy. The numerical data for the fluidic parameters of interest are demonstrated in the tabular form, further few proficient parameters effects like magnetic parameter, Lewis number, stretching rate parameter, the thermal radiation parameter and Prandtl number on velocity, temperature and concentration profiles have been exhibited numerically as well as graphically. By enhancing the velocity slip parameter, increment is examined in temperature and concentration profiles while opposite behavior is recorded in the velocity profile. Both the concentration and temperature profiles decline with the increase in the Stretching rate ratio parameter.

Key-words: *Casson fluid, stretched sheet, velocity slip, reduced Nusselt number, Sherwood number*

Introduction

The rheology of non-Newtonian fluids possess diverse application in industrial sciences and bioengineering particularly petroleum products, geophysics, clay coating, and polymer processing [1-3]. The rhelogy of non-Newtonian Casson fluid has gathered much significance in scientific and engineering areas. Human blood flow can be described using Casson fluid because of the chain construction, the blood cells and the ingredients namely protein, rouleaux and fibrinogen, *etc*. Reddy [4] examined thermal radiation effects for unsteady flow of a non-Newtonian fluid through a stretched sheet. The steady convection flow of a non-Newtonian

* Corresponding author, e-mail: ali.imran@cuiatk.edu.pk

fluid under the effect of uniform temperature was reported by Khalid *et al*. [5]. Akbar [6] used the magnetic effects on peristaltic non-Newtonian nanofluid-flow in the existence of crude-oil refinement. Megahed [7] reported the impact of slip condition for Casson nanofluid based on thin film flow and reported that the parameter of velocity slip reduces the thickness of the flow of thin film. Ibrahim and Makinde [8] discovered the hydromagnetic Casson-nanofluid-flow through a stagnation point and analyzed that increase in the slip parameter, thicknesses of thermal boundary-layers is increased.

In many investigations, fluid-flows are studied by establishing the no-slip at the boundaries, but in some circumstances like foam, suspensions, and emulsions, the no-slip condition at the wall cannot be considered. Nowadays, the phenomenon of slip flow has been extensively investigated by the researchers working on the studies of micro-electro-mechanical systems related to the personification of temperature jump and velocity slip. The nanofluid dynamics for a isothermal stretching sheet with the effects of transpiration by using the homotopy analysis method is implemented by Rashidi *et al*. [9]. The MHD flow of nanofluid past through a stretched surface by implementing partial slip effects and convective boundary has been studied by Rahimi and Freidoonimehr [10]. Tian *et al*. [11] in order to enhance numerical simulation technique for the case super critical pressure fluids, developed a technique by using variant Prandtl number model. Esfe *et al*. [12] with the aid of experimental investigation explored the rheology of TiO_2-MWCNT hybrid nanofluid. Esfe *et al.* [13] in another research paper applied various artificial intelligence methods to forecast the viscosity of TiO_2/SAE 50 nanolubricants with power-law models. Babar and Ali [14] discussed the behavior of hybrid nanofluids with a precise debate on histology, thermophysical properties, synthesis methodologies, future paradigms, current status, and some other salient features. Asadi *et al*. [15] presented the development in the formation techniques and thermophysical axioms, dimensions of oil-based nanofluids and they showed that by adding nanoparticles in a thermal oil, cooling and lubrication productivities could be enhanced. Ilyas *et al.* [16] emphasized on the rheology of nanofluids and they used MWCNT to normalize thermal oil and observed high equilibrium. Esfe, *et al*. [17] capitalized modified non-influenced Sorting Genetic Algorithm to minimize the viscosity and enhance the thermal ability of Al_2O_3-water/EG (20-80) nanofluids. Manasrah, *et al*. [18] focused on the formation of material based on nanoparticles. Almanassra *et al*. [19] carried out investigation in order to compare the impact of various surfactants on the constancy and thermo-physical axioms of nanotubes carbon.

Nesligul *et al.* [20] determined the solution for the position of moving boundary, they modeled the problem using variable space grid method and applied finite element method. Solution for non-linear ODE of non-isothermal fluid transport along with the mass transfer is determined by Kilicman *et al*. [21] by employing homotopy perturbation method. The present work is the numerical treatment for Casson nanofluidic model and the key findings of current investigation can be interpreted in terms of salient features as:

- A mathematical model for 3-D flow of Casson nanofluid over a stretching sheet with chemical reactions, velocity slip, thermal radiation and Brownian motion has been modeled.
- The similarity transformation are exploited to transform the mathematical model in terms of system of ODE and numerical treatment for the dynamics are investigated by the well-established strength of shooting technique.
- Worth of the scheme is endorsed by comparison of results in favorable agreement with state of the art numerical solvers.
- The dynamics of system model is evaluated for reduced Nusselt number, Sherwood number and other proficient parameteric effects for description of the behavior.

Mathematical description of the problem

A 3-D incompressible Casson fluidic problem on the boundary-layer region using heat transfer and thermal radiation effects is modeled in this section. The domain $z > 0$ occupies the flow and sheet has fixed origin and is stretched in two directions. The $u_w x = ax$ and $v_w y = by$ are the respective velocities along the axial and transverse directions. The geometry of the model problem is revealed in fig. 1. The u, v, and w are the velocity components are taken in x-, y-, and z-directions. The T_f and T_∞ represent the surface and ambient temperatures. Furthermore, C_w and C_∞ represent nanoparticles concentration and the ambient concentration of the problem, respectively. The governing equations are given:

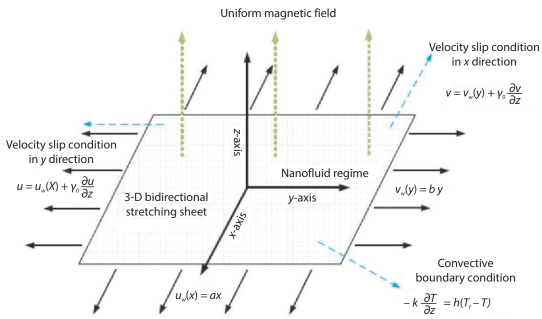

Figure 1. Geometric description of the problem

$$\Delta \mathbf{V} = 0 \tag{1}$$

$$\left(u\frac{\partial}{\partial x}+v\frac{\partial}{\partial y}+w\frac{\partial}{\partial z}\right)u = \nu\left(1+\frac{1}{\beta}\right)\frac{\partial^2 u}{\partial z^2}-\frac{\sigma B^2}{\rho}u \tag{2}$$

$$\left(u\frac{\partial}{\partial x}+v\frac{\partial}{\partial y}+w\frac{\partial}{\partial z}\right)v = \nu\left(1+\frac{1}{\beta}\right)\frac{\partial^2 v}{\partial z^2}-\frac{\sigma B^2}{\rho}v \tag{3}$$

$$\left(v\frac{\partial}{\partial y}+u\frac{\partial}{\partial x}+w\frac{\partial}{\partial z}\right)T = \alpha\left(1+\frac{16\sigma^* T_\infty^3}{3kk^*}\right)\left(\frac{\partial^2 T}{\partial z^2}\right)+\tau\left\{\frac{D_T}{T_\infty}\left(\frac{\partial T}{\partial z}\right)^2+D_B\frac{\partial C}{\partial z}\frac{\partial T}{\partial z}\right\}+ \\ +\frac{Q^*}{(\rho C_p)_f}(T-T_\infty) \tag{4}$$

$$\left(v\frac{\partial}{\partial y}+u\frac{\partial}{\partial x}w\frac{\partial}{\partial z}\right)C = D_B\left(\frac{\partial^2 C}{\partial z^2}\right)-\delta\left(C-C_\infty\right)+\frac{D_T}{T_\infty}\left(\frac{\partial^2 T}{\partial z^2}\right) \tag{5}$$

The respective boundary conditions are expressed:

$$u = u_w\left(x\right)+\gamma_0\frac{\partial u}{\partial z},\ \ v = v_w\left(x\right)+\gamma_0\frac{\partial u}{\partial z},\ \ w = 0,\ -k\frac{\partial T}{\partial z} = h\left(T_f - T\right),\ \ C = C_w at z = 0$$
$$v \to 0,\ \ u \to 0,\ T \to T_\infty,\ \ C \to C_\infty\ z \to \infty$$

The similarity transformations are given:

$$\eta = \left(\frac{\nu}{a}\right)^{1/2} z,\ \ v = ayg'\left(\eta\right),\ \ u = axf'\left(\eta\right),\ \ w = -\sqrt{\nu a}\left[f\left(\eta\right)+g\left(\eta\right)\right]$$

$$\phi\left(\eta\right) = \frac{C-C_\infty}{C_w - C_\infty},\ \ \theta\left(\eta\right) = \frac{T-T_\infty}{T_f - T_\infty}$$

The modeled eqs. (1)-(5) along with the boundary conditions (6) take the following dimensionless form by using the similarity transformation:

$$\left(1+\frac{1}{\beta}\right)f'''(\eta)+\left[f(\eta)+g(\eta)\right]f''(\eta)-\left[f'(\eta)\right]^2-Mf'(\eta)=0 \tag{6}$$

$$\left(1+\frac{1}{\beta}\right)g'''(\eta)+\left[f(\eta)+g(\eta)\right]g''(\eta)-\left[g'(\eta)\right]^2-Mg'(\eta)=0 \tag{7}$$

$$\left(1+\frac{4}{3}Nr\right)\theta''(\eta)+\Pr\left[f(\eta)+g(\eta)\right]\theta'(\eta)+Nb\theta'(\eta)\phi'(\eta)+Nt\left[\theta'(\eta)\right]^2+\Pr Q\theta(\eta)=0 \tag{8}$$

$$\phi''(\eta)+\mathrm{Le}\left[f(\eta)+g(\eta)\right]\phi'(\eta)+\frac{Nt}{Nb}\theta''(\eta)-\mathrm{Le}\chi\phi(\eta)=0 \tag{9}$$

where the magnetic parameter is represented

$$M=\frac{\sigma B_0^2}{a\rho}$$

the Prandtl number

$$\Pr=\frac{\nu}{\alpha}$$

the radiation parameter

$$Nr \qquad \frac{{}^{*}\quad{}_{\infty}^{3}}{k\ k}$$

the Brownian parameter

$$Nb=\frac{\tau D_B\left(C_w-C_\infty\right)}{\nu}$$

the heat generation/absorption factor

$$Q=\frac{Q^*}{a\rho C_p}$$

and the Lewis number

$$\mathrm{Le}=\frac{\nu}{D_B}$$

The respective boundary conditions are:

$$f(0)=g(0)=0,\ f'(0)=1+\gamma f''(0),\ g'(0)=\lambda+\gamma g''(0),\ \theta'(0)=-\mathrm{Bi}\left[1-\theta(0)\right]$$
$$\phi(0)=1,\ g'(\eta)=0,\ f'(\eta)=0,\ \theta(\eta)=0,\ \phi(\eta)=0 \text{ as } \eta\to\infty$$

where

$$\gamma=\gamma_0\left(\frac{\nu}{a}\right)^{-1/2},\ \lambda=\frac{b}{a},\ \mathrm{Bi}=\frac{h}{k}\sqrt{\frac{\nu}{a}}$$

and

$$C_{fx}=\frac{\tau_{wx}}{\frac{\rho_f U_w^2}{2}},\ C_{fy}=\frac{\tau_{wy}}{\frac{\rho_f U_w^2}{2}},\ \mathrm{Nu}_x=\frac{xq_w}{K_f\left(T_f-T_\infty\right)},\ \mathrm{Sh}_x=\frac{xq_m}{D_B\left(C_w-C_\infty\right)}$$

Solution methodology

In this section, a comprehensive description of the numerical procedure used for the solution of the governing, non-linear, non-dimensional eqs. (8)-(11) with respect to boundary conditions (12) has been presented. These dimensionless equations of motions are handled with well known shooting numerical technique. For comparison, the same system of equations are also solved with the help of well known differential equations solver bvp4c. The domain [0, $\eta_{\max}$] is considered for the proposed problem. The value of the $\eta_{\max}$ has been chosen as eight throughout the article. To get first order ODE system, the notations y_1 for f, y_4 for g, y_7 for θ, and y_9 for ϕ are used. The system of equations for the proposed methodology is presented:

$$\begin{aligned}
&y_1' = y_2, \quad y_1(0)=0\\
&y_2' = y_3, \quad y_2(0)=1+\gamma y_3(0)\\
&y_3' = \frac{\beta}{\beta+1}(-y_1y_3 - y_3y_4 + y_2^2 + My_2), \quad y_3(0)=s\\
&y_4' = y_5, \quad y_4(0)=0\\
&y_5' = y_6, \quad y_5(0)=\lambda+\gamma y_6(0)\\
&y_6' = \frac{\beta}{\beta+1}(-y_1y_6 - y_4y_6 + y_5^2 + My_5), \quad y_6(0)=p\\
&y_7' = y_8, \quad y_7(0)=u\\
&y_8' = \frac{1}{1+\frac{4}{3}\mathrm{Nr}}\left[-(y_1+y_4)\mathrm{Pr}y_8 - Nby_8y_{10} - Nty_8^2 - \mathrm{Pr}Qy_7)\right], \quad y_8(0)=-\mathrm{Bi}[1-y_7(0)]\\
&y_9' = y_{10}, \quad y_9(0)=1\\
&y_{10}' = -\mathrm{Le}(y_1+y_4)y_{10} - \frac{Nt}{Nb}y_8' - \mathrm{Le}\chi y_9, \quad y_{10}(0)=w
\end{aligned} \tag{10}$$

where s, p, u, and w are the missing conditions in the initial phase and the stopping criteria for the proposed fluidic problem is considered:

$$\max\left\{\left|y_3\left(\eta_{\max}\right)\right|,\left|y_6\left(\eta_{\max}\right)\right|,\left|y_7\left(\eta_{\max}\right)\right|,\left|y_{10}\left(\eta_{\max}\right)\right|\right\}<\xi \tag{11}$$

where $\xi > 0$ is a small positive number.

An analogy of the presently computed results of $f''(0)$ and $g''(0)$ corresponding to the stretching ratio parameter, λ, and magnetic parameter, M, with those of Hayat *et al*. [22] and Freidoonimehr *et al*. [23] is reflected in tab. 1. The obtained results in tab. 1 are in favorable agreement with the earlier published numerical results.

Table 1. Correlative analysis of present outcomes and with the investigations of Hayat *et al*. [22] and Freidoonimehr *et al*. [23] for $f''(0)$ and $g''(0)$ when γ = Bi = 0

		[22]	[23]	Present	[22]	[23]	Present
λ	M	$-f''(0)$	$-f''(0)$	$-f''(0)$	$-g''(0)$	$-g''(0)$	$-g''(0)$
	0	1	1	1	0	0	0
	1	1.414214	1.414213	1.407219	0	0	0
0.5	0	1.093095	1.093095	1.088232	0.465205	0.465205	0.463325
	1	1.476771	1.476770	1.469457	0.679809	0.679809	0.676445
0.1	0	1.173722	1.173721	1.168172	1.173722	1.173721	1.168172
	1	–	1.535710	1.528099	–	1.535710	1.528099

Results and discussions

Table 2 shows the heat transfer rate rises by enhancing the value of M, the physical parameters Nb, Nt, Le, and Bi while quite different behavior is noted for Nr, the Prandtl number, the chemical reaction parameter, χ, and the stretching rate parameter, λ. However by enhancing the M, the Nb and Le decreases while opposite trend is noticed for the parameters Nr, Pr, Nt, χ, the stretching rate parameter, λ, and the Biot number.

The magnetic parameter effects for both velocity modules (f', g'), temperature, θ, and concentration profiles, ϕ, are shown in figs. 2-5. A drag force known as Lorentz force found to inflict the parameter M for electric conduction. This force is the propensity to slows down the speed of the flowing fluid. Decrements in the velocity profiles are noticed by increasing the magnetic parameter along x- and y-directions. The magnetic parameter is dependent of the Lorentz force as previously mentioned, which works as a proxy in the flow resistance. It is seen that by enhancing the value M, enhancement is noticed in the Lorentz force and as a result, decrement is seen in both the velocity profiles. Furthermore, by enhancing the value of M, increased in the boundary-layer thickness, the concentration profile and thickness of species boundary-layer is recorded. Which clearly reveals that the parameter of magnetic field in the transverse direction clashes with phenomena of transportation. This is significant remark that the huge hurdles in the flow of fluid particles cause heat generation, as a result increment is seen when magnetic field increases. Figure 6 highlighted the parameter Nt impact against the temperature gradient distribution. By increasing the value value of Nt , the molecules are shifted from hot to cooler sur-

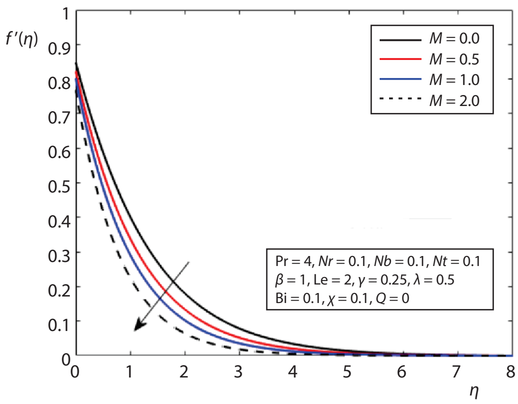

Figure 2. Variants of M for f'

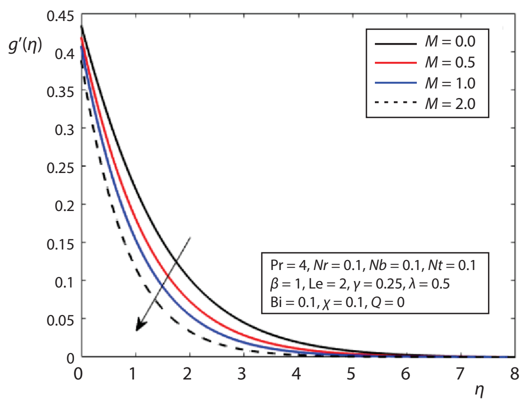

Figure 3. Variants of M for g'

Table 2. Results of the Nusselt and Sherwood number for several parameters.

									$\mathrm{Nu}_x\mathrm{Re}_x^{-1/2}$		$\mathrm{Sh}_x\mathrm{Re}_x^{-1/2}$	
M	Nr	Pr	Nb	Nt	Le	χ	λ	Bi	Shooting	bvp4c	Shooting	bvp4c
0.1	0.1	1	0.1	0.1	0.1	0.1	0.1	1	0.56630	0.56630	0.09801	0.09801
0.5									0.57657	0.57657	0.09078	0.09078
									0.58809	0.58809	0.08162	0.08162
0.5									0.59842	0.59842	0.07264	0.07264
	0.3								0.50168	0.50168	0.17344	0.17344
	0.5								0.45877	0.45877	0.22346	0.22346
	0.7								0.42720	0.42720	0.26035	0.26035
		1.5							0.50427	0.50427	0.17046	0.17046
		2							0.46169	0.46169	0.22012	0.22012
		2.5							0.42977	0.42977	0.25742	0.25742
			0.08						0.56492	0.56492	0.18140	0.18140
			0.06						0.56354	0.56354	0.32037	0.32037
			0.04						0.56217	0.56217	0.59830	0.59830
				0.3					0.57342	0.57342	0.72386	0.72386
				0.5					0.58083	0.58083	1.31462	1.31462
				0.7					0.58854	0.58854	1.86815	1.86815
					0.2				0.56725	0.56725	0.06801	0.06801
					0.3				0.56829	0.56829	0.03236	0.03236
					0.4				0.56939	0.56939	-0.00767	-0.00767
						0.3			0.56542	0.56542	0.14356	0.14356
						0.5			0.56447	0.56447	0.19275	0.19275
						0.7			0.56341	0.56341	0.24621	0.24621
							0.4		0.53208	0.53208	0.12732	0.12732
							0.7		0.50633	0.50633	0.14789	0.14789
							1		0.48560	0.48560	0.16340	0.16340
								1.5	0.66254	0.66254	0.15212	0.15212
								2	0.72389	0.72389	0.18642	0.18642
								2.5	0.76639	0.76639	0.21011	0.21011

face, as a result an enhancement is recorded in the boundary-layer thickness region that leads to rise the temperature profile. The graphical impact of the Lewis number on the concentration of fluid particles is reflected in fig. 7. The Lewis number shows the relation between influence of the rate of thermal and species diffusions in the region along the boundary-layer. To increase the Lewis number, the boundary-layer region involving species are crippled and the temperature profile gets elevated. The velocity slip parameter, γ, effects on the velocity and concentration profiles are illustrated graphically in figs. 8-11. The velocity slip simulation are expressed in eq. (12) that lies between [0, 1]. Presently when $\gamma = 0$, it means it does not obey no-slip condition traditionally. It is recorded that if magnitude of the fluid velocity components is decreased, then

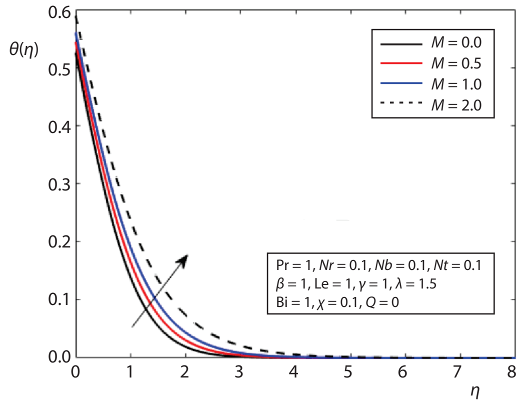

Figure 4. Variants of M for θ

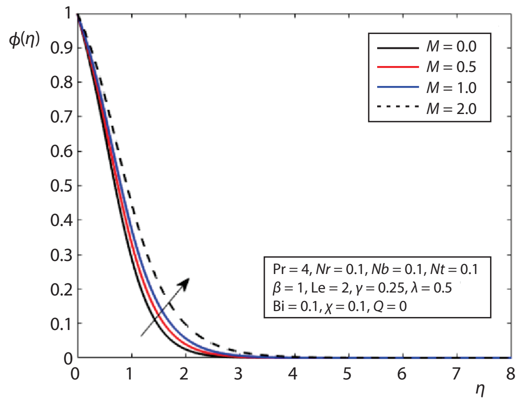

Figure 5. Variants of M for ϕ

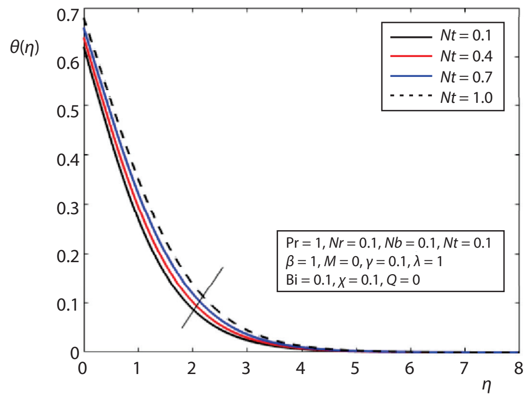

Figure 6. Variants of Nt for θ

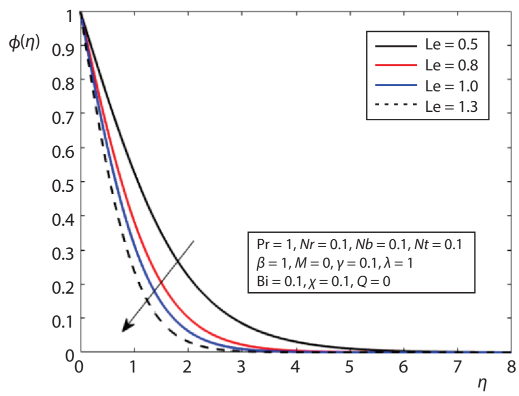

Figure 7. Variants of Le for ϕ

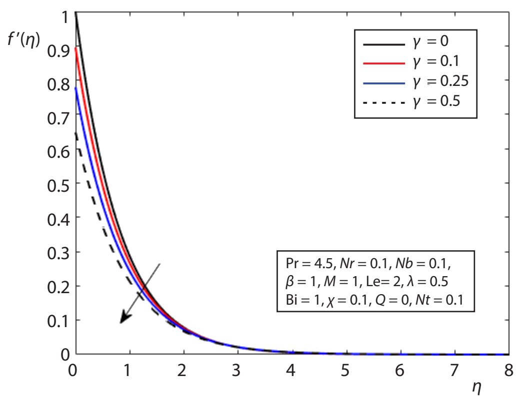

Figure 8. Variants of γ for f'

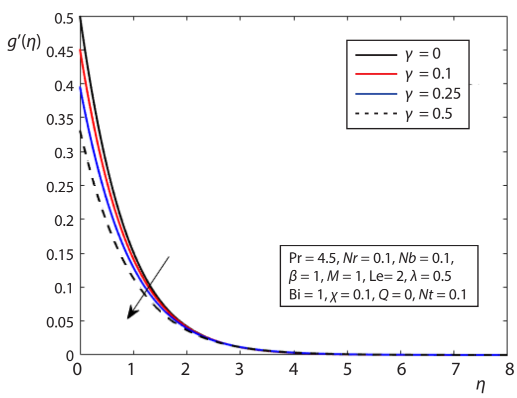

Figure 9. Variants of γ for g'

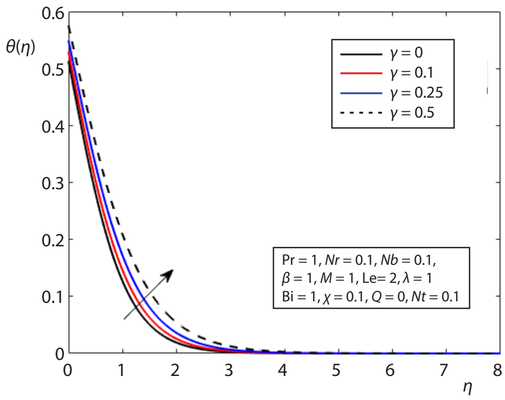

Figure 10. Variants of γ for θ

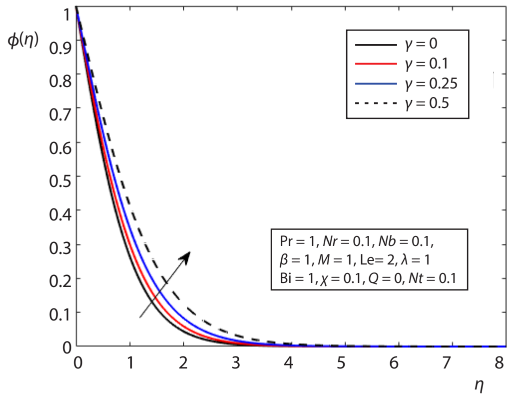

Figure 11. Variants of γ for ϕ

an enhancement is noticed in the temperature and concentration profiles. Moreover, by considering the lesser flow amount and pressed in different directions of the velocity, through this way the slip factor gets solider. However, to increase the velocity slip factor, reduction is noticed through the boundary-level flow in the both axial and transverse directions. Due to this datum, the momentum boundary-layer region thickness is reduced, which results the flow to gets slow down. Similar results are achieved for concentration profile using slip conditions. Stretching rate ratio parameter, λ, effects on temperature distribution and concentration profile are exhibited in figs. 12 and 13. By the definition of the parameter $\lambda = 0$, which signifies the non-bidirectional stretching layer cases. Generally, when the λ exceeds from zero level, the lateral surface transport in the y-direction co-ordinate. Additionally, to enhance the values of the parameter of stretching ratio will reduce the expansion of the region in thermal boundary-layer, which results cooling of the regime, as a result decrement is noticed in the concentration profile and the expansion of region of the species in the boundary-layer.

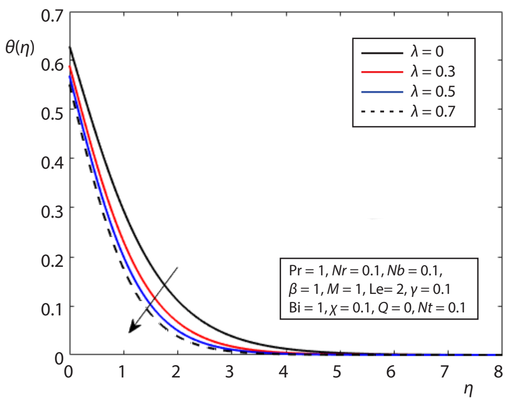

Figure 12. Variants of λ for θ

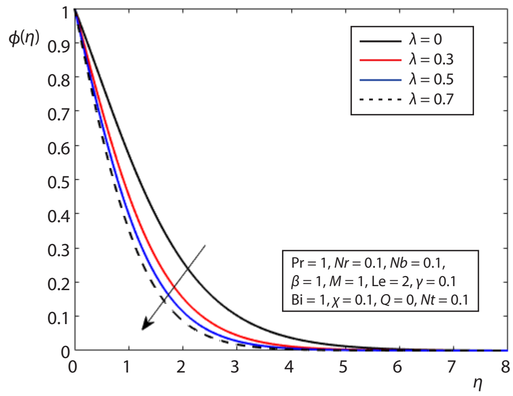

Figure 13. Variants of λ for ϕ

Conclusions

In this study, 3-D flow of Casson nanofluid over a stretched sheet with chemical reactions, velocity slip, thermal radiation and Brownian motion have been analyzed. With the aid of similarity parameters, the system of non-linear PDE are transformed into ODE, which are solved by using shooting method. The numerical outcomes are matched with already established results in the existing literature which show validity of the proposed scheme. The results of present investigated can be summarized as.

- The velocity profiles decreases by enhancing the M and opposite effects have been noticed for temperature profile as well as concentration profile profiles.
- It is observed that by increasing the Nt, the temperature profile decline, on other hand with the increasing value of Lewis number, the concentration profile also decreases.
- By accelerating the velocity slip parameter effects, γ, increment is noticed in temperature and concentration profile while velocity profile decreases.
- Both the concentration and temperature profiles decline with the increase in the stretching rate ratio parameter, λ.

In future, one may explore in stochastic numerical techniques [24-26] to study the dynamics of presented Casson Nanofludic model.

Nomenclature

B_0 – constant magnetic field
Bi – Biot number
C – nanoparticle concentration
C_f – non-dimensional friction coefficient
C_{fx} – skin friction coefficient
C_p – specific heat
C_w – nanoparticle concentration at the wall
C_∞ – concentration at free stream
D – Brownian diffusion coefficient
D_B – mass diffusivity
D_T – thermophoretic diffusion coefficient
$f(\eta)$, $g(\eta)$ – velocity similarity functions
K_0 – chemical reaction coefficient
k – thermal conductivity
Le – Lewis number
M – magnetic parameter
Nb – Brownian motion parameter
Nr – radiation parameter
Nt – thermophoresis parameter
Nu_x – local Nusselt number
Pr – Prandtl number
Q – heat generation/absorption factor
Q_0 – heat generation coefficients
R – auxiliary function
Re – Reynolds number
Sh_x – Sherwood number
T – temperature
T_f – convective surface temperature
T_∞ – ambient temperature
u, v, w – velocity components
x, y, z – rectangular co-ordinates

Greek symbols

α – thermal diffusivity
β – Casson fluid factor
γ – velocity slip parameter
γ_0 – length of slip
χ – chemical reaction factor
ε – total squared residual error
σ – electrical conductivity
λ – stretching rate ratio parameter
ρ – fluid density

References

[1] Esfe, M. H., *et al*., Experimental Investigation on Non-Netonian Behavior of Al_2O_3-MWCNT/5W50 Hybrid Nanolubricant Affected by Alterations of Temperature, Concentration and Shear Rate for Engine Applications, *International Communications in Heat and Mass Transfer*, *82* (2017), Mar., pp. 97-102
[2] Lu, G., *et al*., A Critical Review of Dynamic Wetting by Complex Fluids: from Newtonian Fluids to Non-Newtonian Fluids and Nanofluids, *Advances in Colloid and Interface Science*, *236* (2016), Oct., pp. 43-62
[3] Raju, C. S., Sandeep, N., Heat and Mass Transfer in MHD Non-Newtonian Bioconvection Flow over a Cone/Plate with Cross Diffusion, *Journal of Molecular Liquids*, *215* (2016), Mar., pp. 115-126
[4] Reddy, M. G., Unsteady Radiative-Convective Boundary-Layer Flow of a Casson Fluid with Variable Thermal Conductivity, *Journal of Engineering Physics and Thermophysics*, *88* (2015), 1, pp. 240-251
[5] Khalid, A., *et al*., Exact Solutions for Unsteady Free Convection Flow of Casson Fluid over an Oscillating Vertical Plate with Constant Wall Temperature, *In Abstract and Applied Analysis, 2015* (2015), ID946350
[6] Akbar, N. S., Influence of Magnetic Field on Peristaltic Flow of a Casson Fluid in an Asymmetric Channel: Application in Crude-Oil Refinement, *Journal of Magnetism and Magnetic Materials*, *378* (2015), Mar., pp. 463-468

[7] Megahed, A. M., Effect of Slip Velocity on Casson Thin Film Flow and Heat Transfer Due to Unsteady Stretching Sheet in Presence of Variable Heat Flux and Viscous Dissipation, *Applied Mathematics and Mechanics*, *36* (2015), 10, pp. 1273-1284
[8] Ibrahim, W., Makinde, O. D., Magnetohydrodynamic Stagnation Point Flow and Heat Transfer of Casson Nanofluid Past a Stretching Sheet with Slip and Convective Boundary Condition, *Journal of Aerospace Engineering*, *29* (2015), 2, 04015037
[9] Rashidi, M. M., *et al*., Homotopy Simulation of Nanofluid Dynamics from a Non-Linearly Stretching Isothermal Permeable Sheet with Transpiration, *Meccanica*, *49* (2014), 2, pp. 469-482
[10] Freidoonimehr, N., Rahimi, A. B., Investigation of MHD Nanofluid-Flow over a Stretching Surface with Velocity Slip and Convective Surface Boundary Conditions, *Modares Mechanical Engineering*, *15* (2015), 3, pp. 208-218
[11] Tian, R., *et al*., Study of Variable Turbulent Prandtl Number Model for Heat Transfer to Supercritical Fluids in Vertical Tubes, *Journal Thermal Science*, *27* (2018), 3, pp. 213-222
[12] Esfe, M. H., *et al*., Rheological Behavior Characteristics of TiO_2-MWCNT/10w40 Hybrid Nanooil Affected by Temperature, Concentration and Shear Rate: An Experimental Study and a Neural Network Simulating, *Physica E: Low-Dimensional Systems and Nanostructures*, *94* (2017), Oct., pp. 231-240
[13] Esfe, M. H., *et al*., A Comparison of Performance of Several Artificial Intelligence Methods for Predicting the Dynamic Viscosity of TiO_2/SAE 50 Nanolubricant, *Physica E: Low-Dimensional Systems and Nanostructures*, *96* (2018), Feb., pp. 85-93
[14] Babar, H., Ali, H. M., Towards Hybrid Nanofluids: Preparation, Thermophysical Properties, Applications, and Challenges, *Journal of Molecular Liquids*, *281* (2019), May, pp. 598-633
[15] Asadi, A., *et al*., Recent Advances in Preparation Methods and Thermophysical Properties of Oil-Based Nanofluids: A State-of-the-Art Review, *Powder Technology*, *352* (2019), June, pp. 209-226
[16] Ilyas, S. U., *et al*., Rheological Behavior of Mechanically Stabilized and Surfactant-Free MWCNT-Thermal Oil-Based Nanofluids, *International Communications in Heat and Mass Transfer*, *87* (2017), Oct., pp. 250-255
[17] Esfe, M. H., *et al*., Optimization of Thermophysical Properties of Al_2O_3/water-EG (80:20) Nanofluids by NSGA-II, *Physica E: Low-dimensional Systems and Nanostructures*, *103* (2018), Sept., pp. 264-272
[18] Manasrah, A. D., *et al.*, Surface Modification of Carbon Nanotubes with Copper Oxide Nanoparticles for Heat Transfer Enhancement of Nanofluids, *RSC Advances*, *8* (2018), 4, pp. 1791-1802
[19] Almanassra, I. W., *et al.*, An Experimental Study on Stability and Thermal Conductivity of Water/CNT Nanofluids Using Different Surfactants: A Comparison Study, *Journal of Molecular Liquids*, *304* (2020), Apr., 111025
[20] Nesligul, A. E., An Application of Finite Element Method for a Moving Boundary Problem, *Thermal Science Year*, *22* (2018), Suppl. 1, pp. S25-S32
[21] Kilicman, A., *et al.*, Analytic Approximate Solutions for Fluid-Flow in the Presence of Heat and Mass Transfer, *Thermal Science*, *22* (2018), Suppl. 1, pp. S259-S264
[22] Hayat, T., *et al*., The 3-D Stretched Flow Via Convective Boundary Condition and Heat Generation/Absorption, *International Journal of Numerical Methods for Heat and Fluid-Flow*, *24* (2014), 2, pp. 342-358
[23] Freidoonimehr, N., Rahimi, A. B., Brownian Motion Effect on Heat Transfer of a 3-D Nanofluid-Flow over a Stretched Sheet with Velocity Slip, *Journal of Thermal Analysis and Calorimetry*, *135* (2018), Feb., pp. 207-222
[24] Mehmood, A., *et al*., Design of Neuro-Computing Paradigms for Non-Linear Nanofluidic Systems of MHD Jeffery-Hamel Flow, *Journal of the Tiwan Institute of Chemical Engineers*, *91* (2018), Oct., pp. 57-85
[25] Mehmood, A., *et al*., Intelligent Computing to Analyze the Dynamics of Magnetohydrodynamic Flow over Stretchable Rotating Disk Model, *Applied Soft Computing*, *67* (2018), June, pp. 8-28
[26] Raja, M. A. Z., *et al*., Integrated Intelligent Computing for Heat Transfer and Thermal Radiation-Based Two-Phase MHD Nanofluid-Flow Model, *Neural Computing and Applications*, *32* (2020), Apr., pp. 2845-2877

Paper submitted: June 25, 2019
Paper revised: August 4, 2019
Paper accepted: September 2, 2019